Towards photo-CIDNP MAS NMR as a generally applicable enhancement method

Thamarath Surendran, S.

Chapter 1

Introduction

1.1 *Hyperpolarization methods*

Nuclear magnetic resonance (NMR) spectroscopy is a well known analytical technique which is used to elucidate the structure, dynamics and function of various molecules. NMR is very successful in determining structure and dynamics of small molecules and even proteins in both solution and in the solid state. The value of this technique for providing information on reaction dynamics and for constructing three-dimensional images of proteins is widely accepted. The main drawbacks of this technique are its low sensitivity and its limitation to microsecond time resolution. The unfavorable Boltzmann polarization that occurs at equilibrium conditions is a major reason for the low sensitivity.

In the presence of an external magnetic field, a spin 1/2 is found in either α or β spin orientation. The two states correspond to two energy levels with different energy values of E_α and E_β. In this context the term 'polarization' is used for the nuclear spin polarization, which is the difference of the populations (p_α, p_β) of these two levels. The energy difference ΔE for the transition of a spin from the ground state α to the exited state β depends on the magnetic field $B_{0,}$ according to

$$\Delta E = E_\beta - E_\alpha = \gamma \hbar B_0. \qquad (1.1)$$

In this equation γ represents the gyromagnetic ratio.

The population difference of the two levels for the spin ½ system in thermal equilibrium is governed by the Boltzmann statistics, according to

$$p_\alpha / p_\beta = e^{[\Delta E/kT]}. \qquad (1.2)$$

The term p_α/p_β is the ratio of the populations, which depends on ΔE and on the thermal energy kT. Considering a typical NMR magnet with the magnetic field of 9.4 T (*i.e.*, proton frequency 400 MHz), $\Delta E \sim 10^{-25}$ J. This ΔE is very small compared to transitions in the infrared (10^{-21} J) and the visible region (10^{-19} J). At room temperature, the ratio p_α/p_β is about $e^{0.0001}$, which is close to 1. Hence the population difference between the magnetic energy levels is very small in NMR. Because of this, the probabilities for the absorption of an incident photon or for stimulated emission are similar. The population difference is much larger in visible spectroscopy, in which almost the entire population is in the electronic ground state, and in infrared spectroscopy, in which about 90% of population is in the vibrational ground state. Therefore, and because of the higher photon energy, optical methods are generally more sensitive than NMR. The low sensitivity of NMR causes spectra with weak signal-to-noise ratio. For this reason, large amounts of samples are required. In equilibrium NMR experiments, the sensitivity is optimized by using nuclei with high gyromagnetic ratio, such as ^{1}H. In addition long acquisition times, high magnetic fields, cooled electronics and isotope enriched samples are used to enhance the sensitivity.

An alternative approach for increasing the sensitivity of NMR signals is the creation of non-Boltzmann polarization, so-called "hyperpolarization", which can be expressed as a spin temperature

$$T_s = -h\nu/k \ln(p_\alpha/p_\beta). \qquad (1.3)$$

The T_s can be negative if the nuclear spin states are inverted, corresponding with negative signals in the spectrum.

Several hyperpolarization methods have been developed for increasing the enhancement of NMR signals and their sensitivity. Some of these techniques are dynamic nuclear polarization (DNP),[1,2] optical pumping,[3] optical nuclear polarization,[4] parahydrogen induced polarization,[5,6] chemically induced dynamic nuclear polarization (CIDNP) in liquids[7-9] and in the solid state.[10] Using these hyperpolarization methods, NMR signals can be enhanced by a factor of more than 10000.

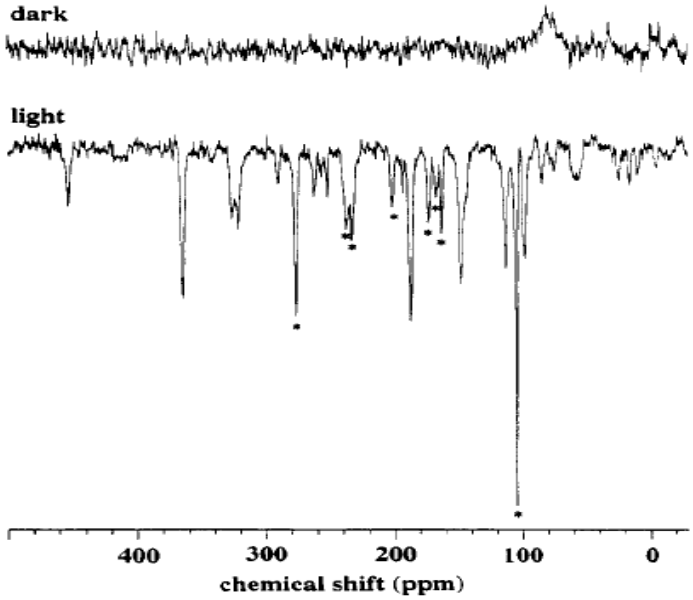

Figure 1.1. The first photo-CIDNP MAS NMR experiment reported in 1994 by Zysmilich and McDermott using ^{15}N labeled RCs of *Rb. sphaeroides* R26 .[10]

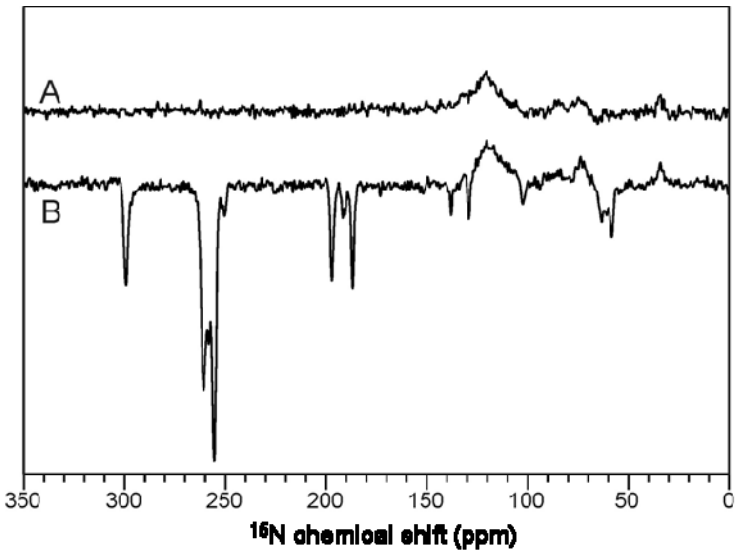

Figure 1.2. ^{15}N MAS NMR spectra of ^{15}N labeled RCs of *Rb. sphaeroides* R26 in the dark (A) and under illumination with continuous white light (B).[11]

1.2 Theory of solid-state photo-CIDNP effect

1.2.1 *Origin of solid-state photo-CIDNP effect*

Photo-CIDNP of dye molecules in solution is a well known hyperpolarization technique,[12,13] which has been discovered in 1967.[7-9] This technique has been explained using the radical pair mechanism (RPM) soon after its discovery.[14,15] In this mechanism, the different chemical fate of the products results in nuclear spin sorting. The origin of photo-CIDNP in liquids relies on the intersystem crossing (ISC) of the spin state of a photoexcited radical pair between the triplet state (T_0) and the singlet state (S) due to coherent S-T_0 mixing. The ISC is primarily due to hyperfine coupling and depends on the nuclear spin states in the radical pair. Thus, the S and T_0 states are correlated to excess and deficiency of the two spin states, respectively. Whether there is an excess of α or β nuclear spin states in the S state of the radical pair depends on the sign of the hyperfine coupling. The radical pair in its singlet state may then recombine to form ground state products. For the radical pair in its triplet state, this process is spin-forbidden, thus it diffuses apart to form escape products. If the products of the two reaction branches have different chemical shifts, nuclear polarization of the same magnitude with different sign induced in singlet and triplet products will be observable in the NMR spectrum. These two contributions of nuclear polarization would cancel each other if singlet and triplet radical pair products have the same chemical fate.

For molecules in solution, photo-CIDNP is observed due to the coupling of the spin dynamics to diffusion and reaction dynamics. Hence such an explanation is insufficient to understand the mechanism of the photo-CIDNP effect in cyclic solid-state reactions. If the nuclear spin longitudinal relaxation rate in singlet and triplet reaction products is different, the RPM can also generate net nuclear polarization. This mechanism is called ‘cyclic reactions’ in liquid-state NMR[16] and ‘differential relaxation’ in solid-state NMR (see below).

The solid-state photo-CIDNP effect is the enhancement of NMR signal intensities in the solid state, where molecular diffusion does not occur.[17,18] This effect was reported for the first time by Zysmilich and McDermott in 1994 in quinone blocked frozen ^{15}N-labeled bacterial reaction centers (RCs) of purple bacteria *Rhodobactor (Rb.) sphaeroides* R26.[10] In this experiment, they observed

strong enhancement of ^{15}N magic-angle spinning (MAS) NMR signals (Figure 1.1). Later, various photosynthetic RCs, as those from *Rb. sphaeroides* wild type (WT),[19] of photosystem I (PSI)[20] and II (PSII),[21-23] as well as of green sulphur bacterial RCs[24] and heliobacterial RCs[25] were analyzed using the photo-CIDNP ^{13}C and ^{15}N MAS NMR technique (for example see Figure 1.2).

An enhancement of a factor of 10000 was observed in ^{13}C photo-CIDNP MAS NMR data collected from bacterial RCs of *Rb. sphaeroides* WT and its carotenoid less mutant R26, in a magnetic field of 4.7 T.[19,26] This very strong enhancement of MAS NMR signals by the solid-state photo-CIDNP effect makes it possible to analyze the photosynthetic RCs in whole photosynthetic systems like chromatophores[25] and cells.[26,27] The solid-state photo-CIDNP effect has been observed in all natural photosynthetic RCs studied so far and it appears to be an intrinsic property of efficient photosynthetic electron transfer. Hence, the effect provides a sensitive analytical technique to study the electronic structure of RCs in great detail. The chemical shifts of the light-induced signals provide information about the electronic structure of the diamagnetic ground state after the photocycle. Similarly, the light-induced signal intensities reveal the electron spin density distribution. In continuous illumination experiments, electron spin density in the p_z orbitals is probed[28] while laser-flash experiments reveal the electron spin densities in the *s*-orbitals.[29]

The mechanism of the solid-state photo-CIDNP effect was explained[17,18,30] following photo-CIDNP MAS NMR studies of quinone depleted or reduced bacterial RCs of *Rb. sphaeroides* WT and R26, in particular on the basis of field-dependent[19,26] and time-resolved experiments.[30] The kinetics and spin dynamics are summarized in Figure 1.3. The primary electron donor (P) of the RC protein is excited to P* by illumination with light. The primary electron donor (P) is a dimer of bacteriochlorophyll (BChl) *a* denoted the "Special pair", whereas a bacteriopheophytin (BPheo) acts as primary electron acceptor (Φ) in RC proteins. From the excited electronic state of the special pair, an electron is transferred to the primary electron acceptor to form a radial pair. Since the excited state is a pure singlet and electron transfer is much faster than coherent evolution, the radical pair is established as a pure singlet (S). In its singlet state is not an eigenstate of the S-

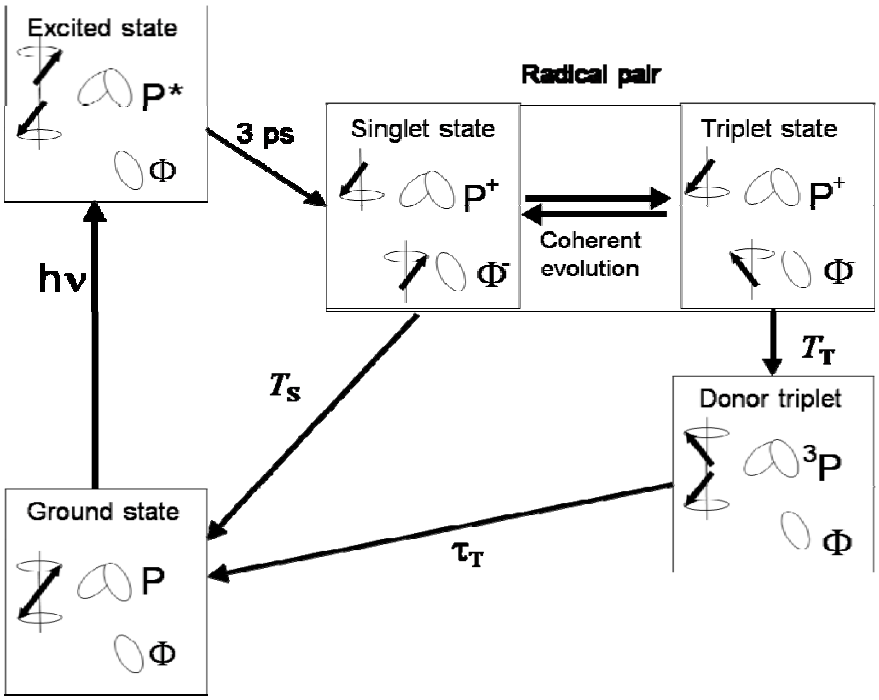

Figure 1.3 Photocycle in quinone-depleted RCs of *Rb. sphaeroides* WT and R26. Upon illumination and fast electron transfer from an excited singlet state, a radical pair is formed in a pure singlet state having high electron spin order. The radical pair is formed by a radical cation at the two donor BChls (Special pair, P) and a radical anion on the BPhe acceptor cofactor (Φ) of the active branch. The chemical fate of the radical pair depends on its electronic spin state: the singlet state is allowed to recombine with the lifetime of T_s = 20 ns and this recombination pathway is termed singlet channel. For the triplet state a direct recombination is spin-forbidden and a donor triplet (^{3}P) is formed with a lifetime of T_T= 1 ns. The lifetime of the donor triplet state (τ_T) is 100 ns for WT RCs and 100 μs for R26 RCs. The recombination pathway of the donor triplet to the ground state is termed triplet channel. Mechanisms building up photo-CIDNP under steady-state conditions are Three spin mixing, Differential decay and Differential relaxation.

T_0 subsystem, this spin-correlated radical pair[31,32] evolves into the triplet state (T_0), or it can decay to the diamagnetic ground state. The formation of the ground-state is a chemical reaction proceeding with the kinetic decay constant T_S. The coherent evolution is controlled by the secular part of the hyperfine interaction A, the coupling of the electrons d, and the difference $\Delta\Omega$ of electron Zeeman interactions between the two electrons and involves the nuclear Zeeman splitting as well.[17] For the triplet state, a direct decay to the ground state is spin-forbidden; therefore it forms a molecular triplet state on the donor (^{3}P). This chemical reaction is

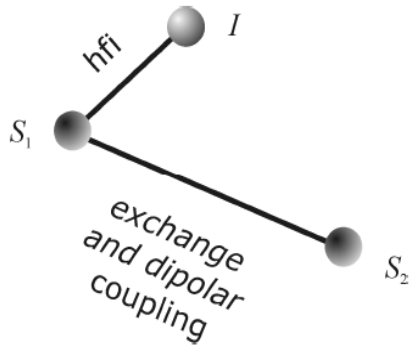

Figure 1.4. The electron-electron- nucleus model system which is used to explain the mechanisms of solid-state photo-CIDNP effect.

described with the kinetic decay constant T_T. The lifetime of the donor triplet state depends on the possibilities for relaxation by coupling to its environment. In WT RCs, the nearby carotenoid provides an excellent relaxation channel, leading to a short lifetime. In the R26 mutant, no carotenoid is available, therefore the ^3P lifetime is significantly longer.

Upon generation of the radical pair in a pure singlet state, perfect electron spin order is created, which is associated with zero-quantum coherence between the $S_{1\alpha}S_{2\beta}$ and $S_{1\beta}S_{2\alpha}$ electron spin states of the radical pair. This zero-quantum coherence is partially transferred into nuclear polarization by two mechanisms, called three-spin mixing (TSM) and differential decay (DD). These two mechanisms run in parallel and explain the emissive pattern of solid state photo-CIDNP NMR signals in the bacterial RCs of *Rb. sphaeroides* WT. In R26 RCs excitation produces a long-lived donor triplet, and differential relaxation (DR) occurs as a third mechanism.[26] These three competing mechanisms, which contribute to the polarization transfer from electrons to nuclei, are explained in detail below.

The solid-state photo-CIDNP effect due to the TSM and DD mechanisms is explained by assuming an electron-electron-nucleus model system (Figure 1.4). This model system consists of two electron spins S_1=1/2, S_2=1/2 and one nuclear spin I=1/2, which is hyperfine coupled to S_1. Since at high magnetic fields, the T_+ and T_- triplet states are energetically too distant to become involved, the spin

dynamics occurs selectively on the S-T_0 subsystem at the zero-quantum transition of the two electron spins (Figure 1.5). In this case, the S-T_0 subsystem can be reduced to an interaction of one nuclear spin I and a fictitious electron spin $S'= ½$.[33] Now, the Hamiltonian of this S-T_0 subsystem is given by[17]:

$$H_{ST0} = \Delta\Omega S_z' + \omega_I I_z + A_{zz} S_z' I_z + A_{zx} S_z' I_x + A_{zy} S_z' I_y - d S_x'. \qquad (1.4)$$

Here $\Delta\Omega$ and ω_I correspond to the electron and nuclear Zeeman interaction respectively. A_{zz} and the $B=(A_{zx}^2 + A_{zy}^2)^{1/2}$ constitute the secular and pseudosecular hyperfine coupling, respectively. The total coupling between the electrons, d, is equal to $2J+d'$. J is the exchange coupling and d' is the dipole-dipole coupling. These parameters and the kinetic constants T_S and T_T (see above) are relevant for the explanation of the photo-CIDNP effect in the solid state by TSM and DD mechanisms.

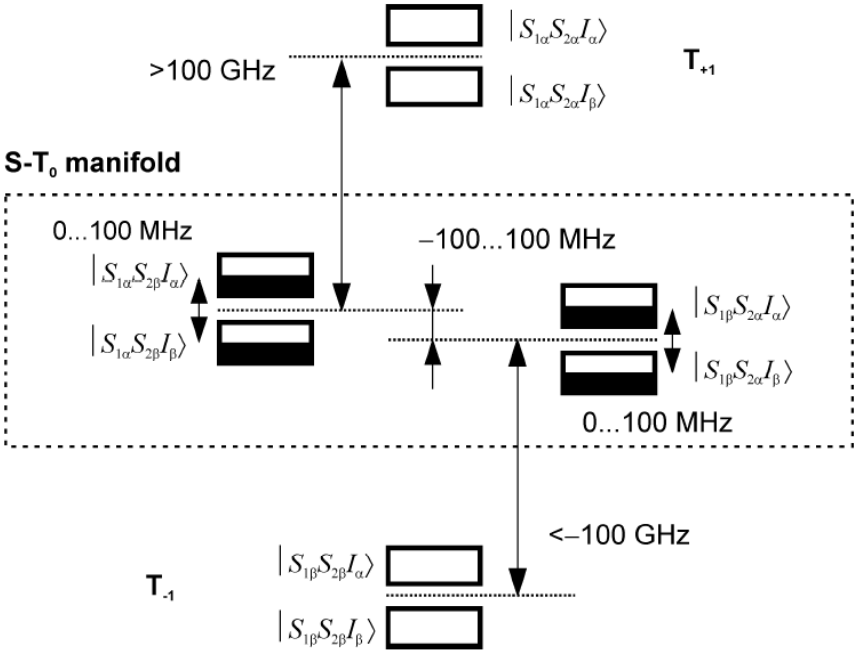

Figure 1.5. The energy levels of the radical pair. According to the Boltzmann distribution, all the spin states are virtually equally populated at thermal equilibrium. Only the singlet (S) state is populated immediately after the photo-induced electron transfer and radical pair formation. During the life time of this radical pair, the S state interconverts to the triplet radical pair T_0 resulting in an S-T_0 subsystem. The difference of the Zeeman interaction of the electron spins, the nuclear Zeeman interaction, hyperfine coupling and the electron-electron coupling are the interactions which split the S-T_0 manifold into four quantum states.

The first three terms in equation 1.4 describe the reaction dynamics according to the RPM, the last three terms are main contributing elements in three-spin mixing. The photo-CIDNP is only active in a small distance range of the radical pair: At this distance the radical pair is subject to mixing while, as often in solution, at shorter or longer distance either the $S_{1\alpha}S_{2\beta}$ and $S_{1\beta}S_{2\alpha}$ or the S and T_0 states become eigenstates and there is no possibility for such mixing.

1.2.2 *Three spin mixing (TSM)*

This pure solid-state mechanism has been proposed by Jeschke in 1997.[33] Here, the anti-symmetry of the coherent spin evolution in the correlated radical pair between the S and T_0 states is broken by state mixing due to B (terms 4 and 5 in equation 1.4) and the electron-electron dipolar coupling (term 6). The symmetry breaking concerning the nuclear states is caused by the B, which tilts the quantization axes of nuclear spins with respect to the external magnetic field. The tilt angles and tilt direction differ in the electron spin $S_{1\alpha}$ and $S_{1\beta}$ manifold. This tilt converts part of the electron-electron zero-quantum coherence that exists in a singlet-born radical pair to electron-electron-nuclear zero/single quantum coherence. A further tilt of the electron spin quantization axes by the exchange coupling or by the electron-electron dipole-dipole coupling converts part of this three-spin coherence into nuclear antiphase coherence. This corresponds to a symmetry breaking with respect to the singlet and triplet state of the radical pair. The antiphase nuclear coherence further evolves to nuclear coherence during the lifetime of the radical pair. On recombination of the pair, part of this coherence is projected to polarizations, since the tilt of the nuclear spin quantization axes due to the pseudo-secular hyperfine field suddenly vanishes.

The TSM gains maximum effect if the double matching condition is fulfilled

$$2\,|\Delta\Omega| = 2\,|\omega_I| = |A|$$

The nuclear polarization by TSM vanishes when the pseudosecular hyperfine contribution approaches zero, $B = (A_{zx}^2 + A_{zy}^2)^{1/2} = 0$, and persists at $\Delta\Omega = 0$ and $A_{zz} = 0$. The contribution of TSM to nuclear polarization is maximum at $\Delta\Omega = 0$.[17] The relevant conditions for TSM are explained in the Figure 1.6. If the double-matching condition is fulfilled, the three lowest energy levels ($S_{1\alpha}S_{2\beta}I_\beta$, $S_{1\beta}S_{2\alpha}I_\alpha$ and $S_{1\beta}S_{2\alpha}I_\beta$) in the S-$T_0$ subsystem are degenerate without the coupling terms $BS_{1z}I_x$ and

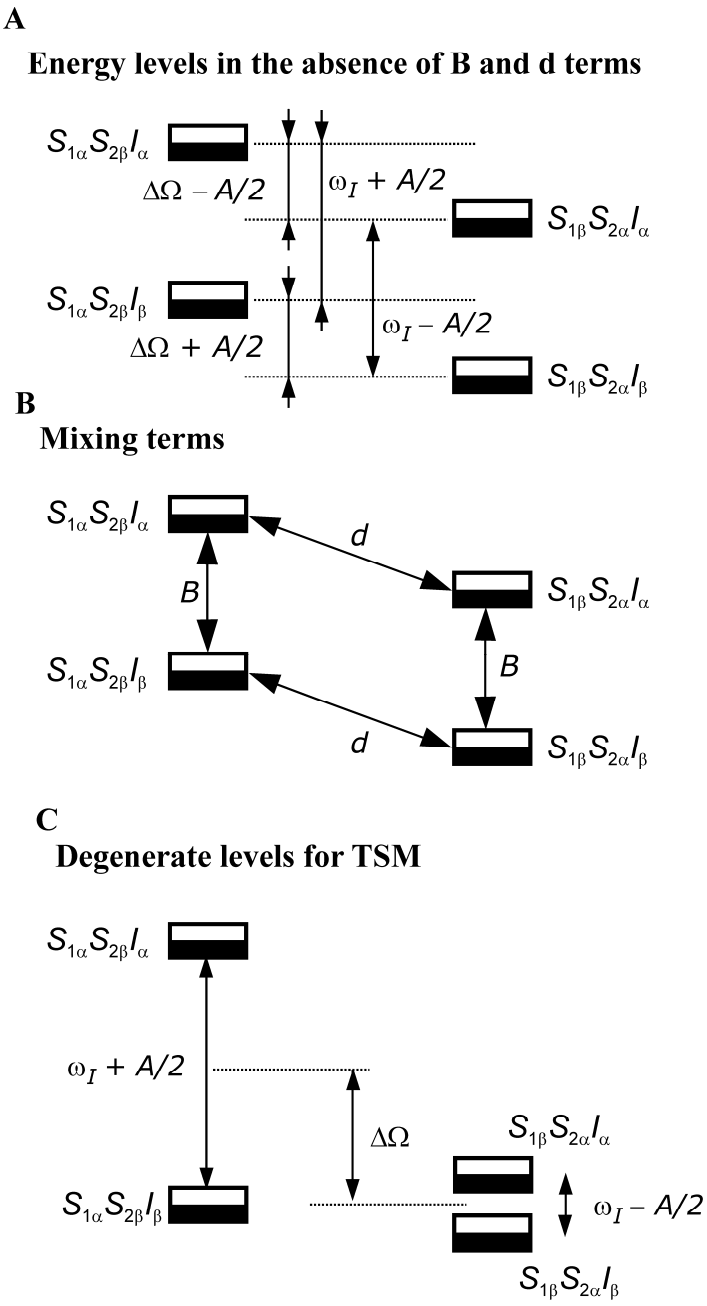

Figure.1.6. (A) Energy levels for the eigenstates according to the first three mutually commuting terms in the fictitious spin representation Hamiltonian (1.4) that provide a basis to describe the S-T_0 manifold. The pseudosecular hyperfine interaction (B) and the electron-electron coupling (d) combine the four quantum base states of the S-T_0 manifold, as indicated in panel (B). In (C) it is indicated how the double matching condition for TSM shifts the base states to produce the degeneracy.

$d(S_{1x}S_{2x}+S_{1y}S_{2y})$. The levels $S_{1\beta}S_{2\alpha}I_{\alpha}$ and $S_{1\beta}S_{2\alpha}I_{\beta}$ are degenerate for $\omega_I = A/2$ and the $S_{1\alpha}S_{2\beta}I_{\beta}$ level becomes degenerate with these two levels if also $\Delta\Omega = \omega_I$. In the initial state all four levels have almost equal initial population and in the absence of the pseudosecular couplings coherence would exist between the left and right pair of levels with the fourth level ($S_{1\alpha}S_{2\beta}I_{\alpha}$) having different energy. Electron electron coupling d splits the two degenerate energy states ($S_{1\alpha}S_{2\beta}I_{\beta}$, $S_{1\beta}S_{2\alpha}I_{\beta}$) that are coherently superimposed and converts the coherence to a transient polarization difference between the two eigenstates. In contrast, the third degenerate ($S_{1\beta}S_{2\alpha}I_{\alpha}$) and the fourth, non-degenerate level ($S_{1\alpha}S_{2\beta}I_{\alpha}$) are only weakly mixed by the electron-electron coupling d and coherence between these two levels can evolve. In addition, the pseudosecular B term of the hyperfine coupling mixes one of the coherently superimposed degenerate levels ($S_{1\beta}S_{2\alpha}I_{\alpha}$) with the third degenerate level ($S_{1\beta}S_{2\alpha}I_{\beta}$). Thus, three of the four levels ($S_{1\alpha}S_{2\beta}I_{\beta}$, $S_{1\beta}S_{2\alpha}I_{\alpha}$ and $S_{1\beta}S_{2\beta}I_{\beta}$) are strongly mixed, while the fourth, non-degenerate level ($S_{1\alpha}S_{2\alpha}I_{\alpha}$) is only weakly admixed. Spin evolution under these conditions leads to partial interconversion between electron-electron zero-quantum coherence and nuclear coherence. When the radical pair recombines, the hyperfine coupling suddenly vanishes, the quantization axis of the nuclear spin changes, and part of the nuclear coherence is converted to nuclear polarization. The contribution to nuclear polarization by the TSM mechanism also depends on the radical pair life times and the coupling d. With very large values of d, this contribution to nuclear polarization becomes negligible, since then the S and T_0 states become eigenstates and evolution of the zero-quantum coherence is blocked. In other words, the fourth level is then also strongly admixed. Hence, photo-CIDNP effect by TSM require moderate coupling between the electrons. In addition, the sign of the photo-CIDNP MAS NMR signals by the TSM contribution depends on the sign of d. Since electron-electron couplings are generally negative, TSM contributions are mostly emissive.[17]

1.2.3 *Differential decay (DD)*

The DD mechanism allows for a solid-state photo-CIDNP effect in the system without relying on the electron-electron coupling d.[34] In this mechanism,

the generation of nuclear polarization from the correlated radical pair state is due to the different lifetimes of singlet (T_S) and triplet radical pairs (T_T). Numerical simulations show that[17] only a single matching of interactions is required for the polarization transfer by the DD mechanism.

$$2\,|\omega_I| = |A_{zz}|$$

Note, however, that the timescales of radical pair recombination and hyperfine-induced spin evolution must also match. Similar to TSM, the Zeeman interaction and the pseudosecular hyperfine interaction *B* are essential for polarization transfer in the DD mechanism. The nuclear polarization by the DD mechanism vanishes if $T_S = T_T$, $\Delta\Omega = 0$, or $A_{zz}=0$. For polarization transfer in photo-CIDNP via the DD mechanism, both the secular part of hyperfine interaction and a difference between *g* values of the two electron spins are required. On the other hand, the DD contribution persists when the electron-electron coupling vanishes ($d=0$). The sign of the DD contribution to nuclear polarization depends on the sign of A_{zz}, $\Delta\Omega$, ω_I and the relative lifetimes of singlet (T_S) and triplet radical pair (T_T).

These two competing mechanisms during radical pair evolution explain the emissive ^{13}C photo-CIDNP MAS NMR signals of *Rb. sphaeroides* WT bacterial RCs. The relative intensity and the chemical shifts of these signals give information about the spin density distribution of the radical pair state and the electronic structure of the ground state, respectively.[19]

1.2.4 *Differential relaxation (DR)*

Bacterial RCs of the R26 mutant of *Rb. sphaeroides* show very similar chemical shifts of photo-CIDNP MAS NMR signals as WT RCs, but the signs of the donor signals are inverted.[26] Here, the contribution to polarization transfer is explained by the DR mechanism. In this mechanism the nuclear polarization is generated similar to the 'cyclic reactions'[16] concept within the radical pair mechanism. The nuclear polarization is created in singlet and triplet branches with the same magnitude and opposite sign, and thus usually cancels in a cyclic reaction. However, nuclear polarization is retained due to different longitudinal nuclear relaxation in both branches.[12] This occurs in the solid state due to hyperfine-induced longitudinal nuclear spin relaxation in the donor triplet state. Relaxation of

the electron spin in the triplet state modulates the hyperfine field at the nucleus, which in turn causes stochastic transitions between nuclear spin states. The mechanism is termed differential relaxation (DR) mechanism.

The R26 mutant has a long living donor triplet that is not rapidly quenched by *e.g.* a carotenoid co-factor near to the special pair P as in the corresponding WT.[42] During this long lifetime of the donor triplet (τ=100 μs), when compared to that in WT (τ=100 ns), a part of triplet born polarization is relaxed. The difference of the photo-CIDNP MAS NMR spectra of *Rb. sphaeroides* WT and R26 RCs is explained by this mechanism.[35,36] Since the DR mechanism relies on relaxation induced by a stochastically fluctuating hyperfine field in the donor triplet state, the relative line intensities of the photo-CIDNP MAS NMR signals can provide information about the electron spin density distribution in the donor triplet state.

1.3 *Photo-CIDNP MAS NMR set-up*

1.3.1 *Setup for continuous illumination photo-CIDNP MAS NMR.*

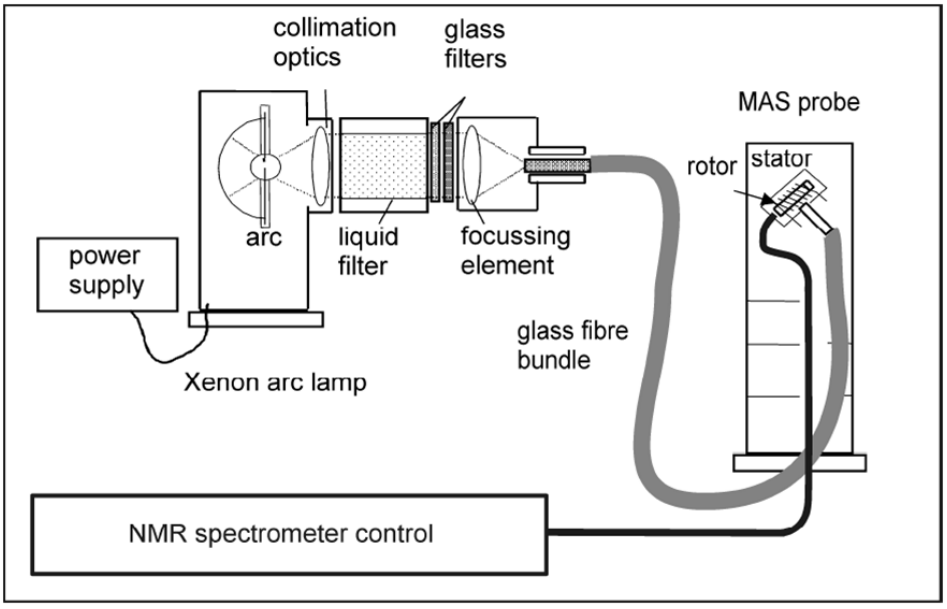

Figure 1.7: The setup for continuous illumination photo-CIDNP MAS NMR experiments

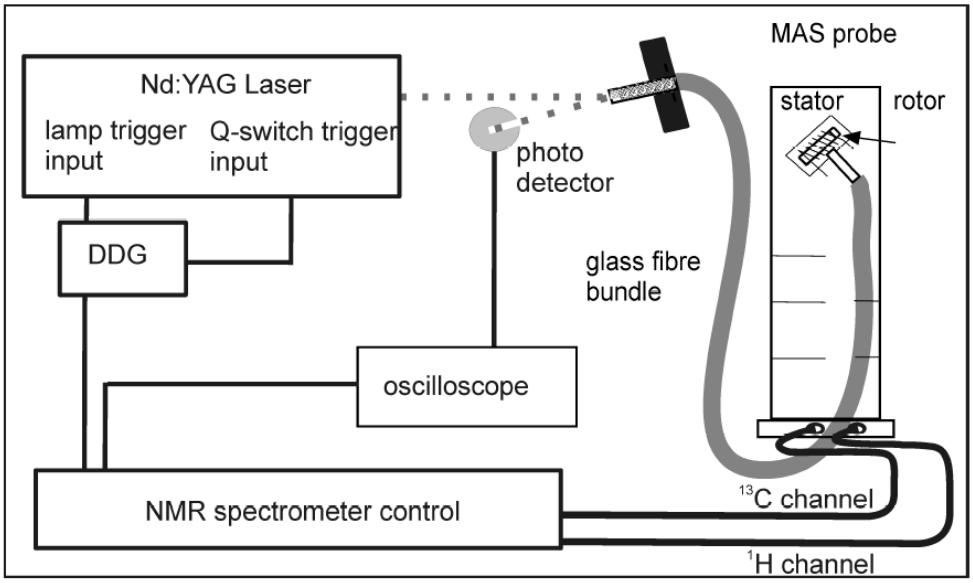

Figure 1.8. The setup for time resolved photo-CIDNP MAS NMR experiments.

Figure 1.7 shows the setup for continuous illumination photo-CIDNP MAS NMR experiments. For illumination of the sample, a 1000 W xenon arc lamp equipped with collimation optics, liquid filter and glass filters is used. The sample is illuminated with radiation similar to sunlight, which includes the range from UV to IR. The IR radiation is filtered using liquid and glass filters. An optical fiber is used to connect the illumination setup to the sample and it is attached to the stator of the MAS NMR probe. The probe was already modified for getting proper illumination from the side and the changes include (a) a bore drilled into the upper partition plate which separates the electronics and stator; (b) a small opening made in the stator to illuminate the sample; and (c) a coil wound from thin silver wire. Transparent sapphire rotors are generally used for allowing a homogeneous illumination of the sample. The Hahn echo pulse sequence[37] with two-pulse phase modulation (TPPM) proton decoupling[38] is used for collecting continuous illumination photo-CIDNP MAS NMR spectra.

1.3.2 *Laser setup for time-resolved photo-CIDNP MAS NMR*

A nano-second laser setup is used for time resolved photo-CIDNP MAS NMR studies for getting information about the electronic structure of RCs at atomic resolution. The laser setup shown in the Figure 1.8 consists of a laser with a 15 Hz repetition rate at 532 nm. This wavelength is opted for because green light gives maximum penetration to optically dense samples. A digital delay generator (DDG) is used to trigger the pump lamps, exciting both the Nd:YAG crystal and the laser Q-switch. The DDG is connected to the NMR spectrometer control that provides the triggering impulse by NMR pulse programming. A fiber aligner is used to fix the multimode optical light fiber. Laser pulses with pulse widths of 6-8 ns and energies between 20-270 mJ were produced. A 500 MHz oscilloscope, which is connected to the ^{13}C channel of the spectrometer and to the homemade photo detector, checks the timing between the laser pulse and the NMR pulse. The photo-detector consists of a fast photo-diode and a custom made amplifier. The laser pulses are transferred to the sample by a multimode optical fiber, attached to the stator of MAS NMR probe.

The same NMR pulse sequence for continuous illumination experiments is used for time resolved experiments with some modifications.[39] Additional ^{13}C presaturation pulses are applied prior to each laser pulse to destroy any polarization from previous laser flashes. Due to the destruction of this primary polarization by ^{13}C presaturation pulses, the recycle delay can be reduced to ~200 ms compared to the recycle delay of ~4 s in steady state experiments.[39]

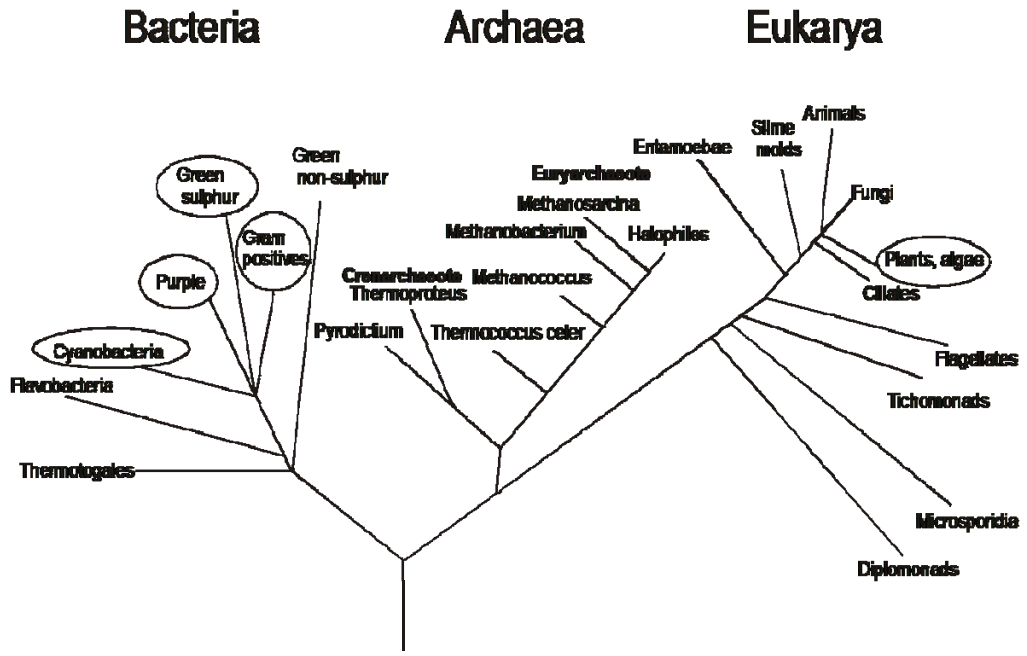

Figure 1.9. This figure shows the phylogenetic tree based on the small subunit RNA method. The photo-CIDNP MAS NMR is active in the photosynthetic organisms that are encircled.

1.4 *Applications of the solid state photo-CIDNP effect*

The solid state photo-CIDNP effect is proven to be an efficient method to analyze the electronic structure of cofactors in the RC proteins of different photosynthetic organisms. The combination with different isotope labeling methods adds further to selectivity and sensitivity. New developments as two-dimensional photo-CIDNP MAS NMR and nano-second flash photo-CIDNP MAS NMR allow exploring not only the aromatic cofactors, but also their surroundings in the protein binding pocket. The maximum enhancement of MAS NMR signals was observed in a magnetic field of 4.7 T.[19,26] Over the years, it was found that the solid state photo-CIDNP effect occurs in all tested phyla of photosynthetic organisms (Figure 1.9). It thus appears that this effect is an intrinsic property of natural photosynthetic systems.[40] Solid-state photo-CIDNP MAS NMR has been developed into a fully operational analytical method to study structure and function of different RCs in various photosynthetic organisms.

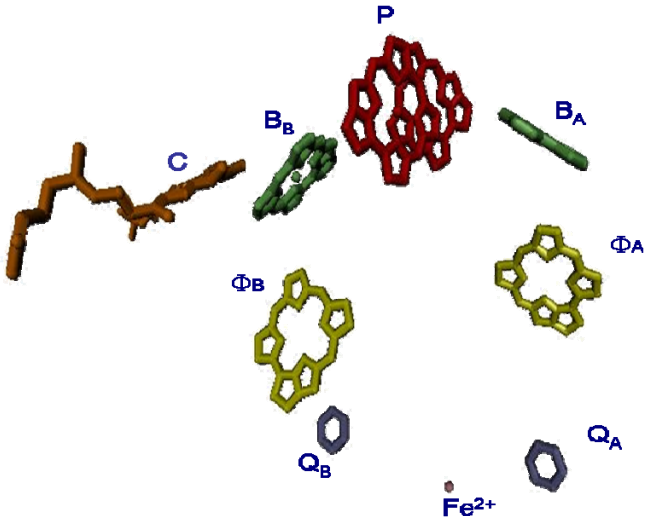

Figure 1.10: The cofactor arrangement in RCs of *Rb. sphaeroides* WT.

1.4.1 *Purple bacteria Rb. sphaeroides WT and R26.*

Rb. sphaeroides WT are anaerobic photosynthetic bacteria consisting of a photosynthetic apparatus with photosynthetic RC proteins and two light harvesting (LH) complexes, LH1 and LH2. The sunlight is captured by these LHs, which transfer the excitation energy to the RC.[41] The RC is a transmembrane protein complex in which the light (L) and medium (M) polypeptides subunits bind the cofactors. The cofactors of RC proteins consist of a well-interacting homodimer of BChl *a* molecules, two non-interacting BChl *a*, two BPheo *a* molecules, two ubiquinone-10 (Q) molecules, a non-heme iron (Fe^{2+}) and a carotenoid molecule. These cofactors are arranged in two branches, the active A branch and the inactive B branch. The homodimer of BChl *a* forms a special pair P, which is the primary electron donor. The other BChl *a* molecules are located on either side of the special pair and function as accessory pigments (B_A and B_B). The primary electron acceptor BPheo *a* molecules (Φ_A and Φ_B) are situated below the special pair in Figure 1.10. The quinones Q_A and Q_B are located below this and finally the Fe^{2+} is placed at the center of the two branches. The carotenoid that is placed near B_B breaks the symmetry of this cofactor arrangement. This carotenoid is absent in the RC of the mutant strain, *Rb. sphaeroides* R26.

Even though the RC protein has a symmetric structure, the electron transfer pathway is asymmetric and charge separation proceeds selectively through the A branch.[42] The special pair P of the RC is formed by two BChl *a* cofactors P_L and P_M, corresponding to the polypeptide chains to which they are attached. The asymmetry of the special pair P in its radical cation state has been investigated by experimental techniques like EPR, ENDOR, TRIPLE resonance studies etc. These studies reveal excess electron density in P_L compared to P_M.[43-45] This asymmetry has been attributed to a different packing structure for the two BChls in P_L and P_M, in combination with other effects of the environment around the special pair.[43] These experimental techniques have not been able to provide information about the ground state electronic structure of the special pair. Photo-CIDNP MAS NMR on site specific ^{13}C labeled RCs of *Rb. sphaeroides* WT is the only technique which has provided insight into the ground state electronic structure of the special pair.[19] Moderate differences in the electronic structure between the two BChl molecules of the special pair in the electronic ground state are observed by photo-CIDNP ^{13}C MAS NMR chemical shifts. This difference was attributed to hydrogen bonding of one of the BChl molecules.[46] The delocalisation of a major fraction of the electron spin density over the two BChl molecules of the special pair and the photochemically active BPhe is also confirmed from these experiments.[46] Photo-CIDNP MAS NMR shows very strong enhancement of NMR signals from the RCs of *Rb. sphaeroides* WT. These experiments revealed that the electron spin density ratio of special pair cofactors P_L and P_M is 3:2 in the radical cation state.[19] This is well in agreement with the ENDOR data.[43]

The photo-CIDNP MAS NMR spectrum was also observed in RCs of the carotenoid less mutant *Rb. sphaeroides* R26 and showed sign inversion for light induced signals in the region 170-130 ppm caused by the DR mechanism.[26] The magnetic field dependence of photo-CIDNP MAS NMR was also investigated in RCs of *Rb. sphaeroides* R26 and showed maximum enhancement in a magnetic field of 4.7 T.[26] This strong enhancement allows for 2-dimensional photo-CIDNP MAS NMR experiments on different site-directed ^{13}C labeled RCs of *Rb. sphaeroides* WT. The RFDR or PDSD pulse sequences, for example, in which the cross polarization pulse is replaced by $\pi/2$ pulse, were applied in 2-d experiments.

Chemical shift assignments of light induced signals from the special pair, accessory chlorophylls and BPheo *a* of the RCs have been obtained.[47] The time-resolved photo-CIDNP MAS NMR experiments on RCs of *Rb. sphaeroides* WT and R26 have been performed allowing for detailed understanding of the mechanism of the solid-state photo-CIDNP.[30] These experiments also provide information about the true electron spin densities at atomic resolution and help to elucidate the spin dynamics of the spin correlated radical pair at the microsecond timescale.[29]

1.4.2 *Rhodopseudomonas acidophilia* (*Rps. acidophilia*)

As for *Rb. sphaeroides*, *Rps. acidophilia* is also belonging to the family of purple bacteria. The solid-state photo-CIDNP effect was observed in ^{13}C labeled LH1-RC complexes of *Rps. acidophilia*.[48] It was detected by light induced ^{13}C MAS NMR signals in the aromatic region of the spectrum. Light induced ^{13}C MAS NMR data collected from *Rps. acidophilia* show the emissive signals very similar to those in *Rb. sphaeroides* WT RCs. Both of them have a similar distribution of electron spin density in the radical pair state.

1.4.3 *Green Sulphur bacteria: Chlorobium tepidum (C. tepidum)*

The green sulfur bacterium *C. tepidum* is an anoxygenic photosynthetic species with type I RCs.[49,50] The cofactors of the RC protein comprise eight molecules of BChl *a*, two Chl *a* molecule derivatives and carotenoids.[51,52] The primary electron donor is the homodimer of BChl *a*[52,53] and a derivative of a Chl *a* molecule acts as the primary electron acceptor.[54] The Fe-S clusters act as terminal electron acceptors.[55] The solid state photo-CIDNP effect was observed in purified FMO-RC particles of *C. tepidum*.[24] It was detected by light induced ^{13}C MAS NMR signals. The photo-CIDNP MAS NMR spectrum of *C. tepidum* shows an emissive light induced spectrum that is comparable to data obtained from *Rb. sphaeroides* WT RCs.

1.4.4 *Heliobacteria Heliobacillus mobilis (Hb. mobilis)*

Hb. mobilis, strictly anaerobic photosynthetic bacteria, are present mainly in rice paddy fields of Thailand. *Hb. mobilis* has less complex RCs and the RCs and the antennae pigments are bound to a single pigment protein complex, which is embedded in cytoplasmic membranes.[56] *Hb. mobilis* is also characterized by the presence of unique BChl *g* pigments. The primary electron donor in heliobacterial RCs is the homodimer of BChl *g*.[57,58] BChl *g* also act as antennae pigments. The primary electron acceptor is 8'-hydroxy Chl *a*.[59] The RCs of *Hb. mobilis* belong to the class of type I RCs, which possess Fe-S clusters as terminal electron acceptors.[60,61] The ^{13}C photo-CIDNP MAS NMR spectrum was observed in isolated membrane fragments of *Hb. mobilis*.[25] The photo-CIDNP spectrum shows light induced absorptive and emissive signals reminiscent of those obtained from RCs of *Rb. sphaeroides* R26. It was assumed that the positive signals were coming from the primary electron donor BChl *g* and the negative signals from the electron acceptor 8^1-hydroxy Chl *a*.[25]

1.4.5 *Plants and cyanobacteria*

In plants and cyanobacteria, the RCs possess a similar basic structure and are located in the photosynthetic membrane. They have the most complex photosynthetic systems in which both PSI and PSII can drive the light induced electron transfer simultaneously. PSI belongs to the type I RCs which have Fe-S clusters as terminal electron acceptors. In PSI, the cofactors for electron transfer are arranged in two branches which include six chlorophylls, two phylloquinones and three iron sulphur clusters.[62] The first pair, the heterodimer of Chl *a* and its epimer acts as a primary electron donor called P700 which is a strong reducing agent and the next pair of Chl *a* acts as accessory pigments. The primary electron acceptor is the third pair of Chl *a*. The phylloquinones act as secondary electron acceptors. The oxidation of water to oxygen is done by PSII in which the oxidized primary electron donor $P680^{\bullet+}$ is a strong oxidizing agent. The RC complex contains two subunits D_1 and D_2 and the cofactors are arranged in two branches.[63,64] This arrangement consists of a pair of Chl *a* molecules P_{D1} and P_{D2} and are followed by two other Chl *a* molecules. The two pheophytins, $Pheo_{D1}$ and $Pheo_{D2,}$ are also

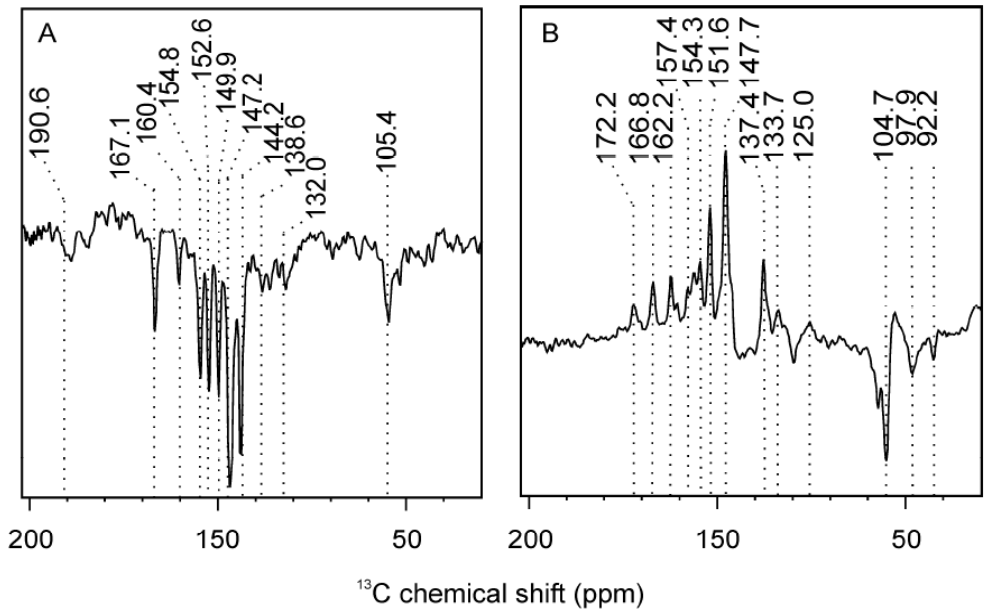

Figure 1.11. ^{13}C photo-CIDNP MAS NMR spectra of (A) PSI and (B) PSII at the magnetic field of 9.4 T and spinning frequency of 9 kHz.

present. PS II belongs to the type II RCs which have two plastoquinones. These plastoquinones act as terminal electron acceptors. The differences in electronic structure and redox properties of both photosystems in plants are yet to be fully understood.[65-67]

The solid-state photo-CIDNP effect was observed in RC preparations of PSI and PSII and detected by the huge enhancement of ^{13}C MAS NMR signals (Figure 1.11). The ^{13}C photo-CIDNP spectra of PSI preparations show emissive signals comparable to *Rb. sphaeroides* WT RCs.[20] The emissive and absorptive patterns of ^{13}C photo-CIDNP MAS NMR signals in PSII preparations are similar to those in *Rb. sphaeroides* R26 RCs.[21,22] In the photo-CIDNP spectrum of PSI, all signals are assigned to a donor cofactor Chl *a*. In PSII, the absorptive signals are assigned to a Chl *a* donor cofactor and the additional emissive signals assigned to an axial histidine that interacts with the donor. The intensities of the light induced signals in the PSII spectrum reveal the distribution of electron spin density over the donor. The difference with monomeric Chl *a* in solution is explained by the shifting of charge towards the pyrrole rings III/IV of the donor Chl *a* due to its interaction with an axial histidine.[23] This also might relate to the extraordinary redox potential

of the $P680^{\bullet+}$. The photo-CIDNP studies in PSI and PSII show that the primary electron donor of PSI is the radical cation of P700 which appears to be an undisturbed cofactor Chl *a*.[20]

1.5 *Scope of the thesis*

The central issue of the thesis addresses a fundamental problem of solid state NMR spectroscopy: The increase of sensitivity and selectivity of NMR, *i.e.* to develop and improve spin-hyperpolarization methods. Various hyperpolarization methods have been developed for this purpose. One such method is the photo-CIDNP MAS NMR, a nuclear hyperpolarization method induced by photo-chemical reactions.

The photo-CIDNP MAS NMR was observed in the membrane fragments of heliobacteria *Hb. mobilis*. Photo-CIDNP MAS NMR studies on entire cells of heliobacteria *Hb. mobilis* are presented in ***Chapter 2***. RCs of *Hb. mobilis* photoisomerize to the aerobic form in the presence of oxygen. Both anaerobic and aerobic forms of *Hb. mobilis* cells are analyzed here using photo-CIDNP MAS NMR. It is remarkable that the electron transfer, the symmetric nature and the kinetics of the RCs in both forms can be resolved with the help of the photo-CIDNP MAS NMR technique, even though the X-ray structures of heliobacterial RC are not available. This chapter also demonstrates that photo-CIDNP MAS NMR can be applied as an analytical tool directly on the cellular level. It implies that this hyperpolarization method can be applied to cells and bacteria even if no further purification is known or possible.

To improve the knowledge of the solid-state photo-CIDNP effect, field dependencies are measured over large ranges (***Chapter 3***). The maximum enhancement of the photo-CIDNP MAS NMR effect is determined to be at the magnetic field of 4.7 T and it is a factor of about 10000 in the RCs of *Rb. sphaeroides* WT and R26. This matching optimum is well explained with the TSM and DD as the constituting mechanisms. For R26 RCs, the photo-CIDNP MAS NMR effect increases significantly below 4.7 T. Experimental observations, computer simulations and theoretical predictions are used to describe the effect in terms of the DR. The analysis of the DR allows constructing the electron spin

density distribution in the ^{3}P donor triplet state. Hence, another mechanism with another analytical aspect stresses the versatility of photo-CIDNP MAS NMR as hyperpolarization method.

Chapter 4 describes the first observation of photo-CIDNP MAS NMR in phototropin LOV1-C57S, overcoming an old limitation of the method. Until now, the photo-CIDNP MAS NMR has been restricted only to natural photosynthetic RCs. ***Chapter 5*** provides the first analytical studies on the LOV1 system. The observation underlines the potential to develop photo-CIDNP MAS NMR into an enhancement method generally applicable to electron transfer proteins. In ***Chapter 6*** this leads to a new paradigm, expecting plenty of photo-CIDNP hyperpolarization if the experiment is optimized for the LOV1 system.

References

(1) Griffin, R. G.; Prisner, T. F. *Phys. Chem. Chem. Phys.* **2010**, *12*, 5737-5740.

(2) Leggett, J.; Hunter, R.; Granwehr, J.; Panek, R.; Perez-Linde, A. J.; Horsewill, A. J.; McMaster, J.; Smith, G.; Kockenberger, W. *Phys. Chem. Chem. Phys.* **2010**, *12*, 5883-5892.

(3) Kastler, A. *Science* **1967**, *158*, 214-21.

(4) Maier, G.; Haeberlen, U.; Wolf, H. C.; Hausser, K. H. *Phys. Lett.* **1967**, *25A*, 384-385.

(5) Bowers, C. R.; Weitekamp, D. P. *Phys Rev Lett* **1986**, *57*, 2645-2648.

(6) Bowers, C. R.; Weitekamp, D. P. *J. Am. Chem. Soc.* **1987, *109,*** 5541-5542.

(7) Bargon, J.; Fischer, F.; Johnsen, U. *Z. Naturforsch.* **1967**, *A 22*, 1551-1555.

(8) Bargon, J.; Fischer, H.; *Z. Naturforsch.* **1967,** *A 22*, 1556-1562.

(9) Ward, H. R.; Lawler, R. G. *J. Am. Chem. Soc.* **1967**, *89*, 5518.

(10) Zysmilich, M. G.; McDermott, A. *J. Am. Chem. Soc*. **1994**, *116*, 8362-8363.

(11) Prakash, S.; Tong, S. H.; Alia, A.; Gast, P.; Jeschke, G.; Matysik, J. in Photosynthesis: Fundamental Aspect to Global Perpectives, (A. ed. by van der Est, A. Bruce), Allen Press Montreal, pp. 236-237, (**2005**).

(12) Hore, P. J.; Broadhurst, R. W. *Progr. NMR Spectrosc.* **1993**, *25*, 345-402.

(13) Goez, M. (1997) *Photochemically induced dynamic nuclear polarization* In Advances in photochemistry, (eds. Neckers, D. C; Volman, D. H; von Bülau, G.) Wiley, New York, *Volume 23*, pp 63-163.

(14) Closs, G. L.; Closs, L. E. *J. Am*. *Chem*. *Soc*. **1969**, *91*, 4549-4550.

(15) Kaptein, R.; Oosterhoff, J. L. *Chem*. *Phys*. *Lett*. **1969**, *4*, 195-197.

(16) Closs, G. L. *Chem*. *Phys*. *Lett*. **1975**, *32*, 277-278.

(17) Jeschke, G.; Matysik, J. *Chem. Phys.* **2003***, 294***,** 239-255.

(18) Daviso, E.; Jeschke, G.; Matysik, J. in Biophysical Techniques in Photosynthesis II (Aartsma T.J., Matysik, J., eds.), Springer Dordrecht, pp. 385-399 (**2008**).

(19) Prakash, S.; Alia; Gast, P.; de Groot, H. J.; Jeschke, G.; Matysik, J. *J. Am. Chem. Soc.* **2005**, *127*, 14290-8.

(20) Alia; Roy, E.; Gast, P.; van Gorkom, H. J.; de Groot, H. J.; Jeschke, G.; Matysik, J. *J Am Chem Soc* **2004**, *126*, 12819-26.

(21) Matysik, J.; Alia; Gast, P.; van Gorkom, H. J.; Hoff, A. J.; de Groot, H. J. *Proc. Natl. Acad. Sci. U. S. A* **2000**, *97*, 9865-70.

(22) Diller, A.; Alia; Roy, E.; Gast, P.; van Gorkom, H. J.; Zaanen, J.; de Groot, H. J.; Glaubitz, C.; Matysik, J. *Photosynth Res* **2005**, *84*, 303-8.

(23) Diller, A.; Roy, E.; Gast, P.; van Gorkom, H. J.; de Groot, H. J.; Glaubitz, C.; Jeschke, G.; Matysik, J.; Alia, A. *Proc. Natl. Acad. Sci. U. S. A.* **2007**, *104*, 12767-71.

(24) Roy, E.; Alia; Gast, P.; van Gorkom, H.; de Groot, H. J.; Jeschke, G.; Matysik, J. *Biochim Biophys Acta* **2007**, *1767*, 610-5.

(25) Roy, E.; Rohmer, T.; Gast, P.; Jeschke, G.; Alia, A.; Matysik, J. *Biochemistry* **2008**, *47*, 4629-35.

(26) Prakash, S.; Alia, A.; Gast, P.; de Groot, H. J.; Matysik, J.; Jeschke, G. *J. Am. Chem. Soc.* **2006**, *128*, 12794-9.

(27) Janssen, G. J.; Daviso, E.; van Son, M.; de Groot, H. J.; Alia, A.; Matysik, J. *Photosynth Res*, *104*, 275-82.

(28) Diller, A.; Prakash, S.; Alia, A.; Gast, P.; Matysik, J.; Jeschke, G. *J Phys Chem B* **2007**, *111*, 10606-14.

(29) Daviso, E.; Prakash, S.; Alia, A.; Gast, P.; Neugebauer, J.; Jeschke, G.; Matysik, J. *Proc Natl Acad Sci U S A* **2009**, *106*, 22281-6.

(30) Daviso, E.; Alia, A.; Prakash, S.; Diller, A.; Gast, P.; Lugtenburg, J.; Jeschke, G.; Matysik, J. *J. Phys. Chem. C* **2009**, *113*, 10269-10278.

(31) Hore, P. J.; Hunter, D. A.; McKie, C. D.; Hoff, A. J. *Chem. Phys. Lett.* **1987**, *137*, 495-500.

(32) Closs, G. L.; Forbes, M. D. E.; Norris, J. R. *J. Phys. Chem.* **1987**, *91*, 3592-3599.

(33) Jeschke, G. *J. Chem. Phys.* **1997**, *106*, 10072-10086.

(34) Polenova, T.; McDermott, A. E. *J. Phys. Chem. B* **1999**, *103*, 535-548.

(35) Goldstein, R. A.; Boxer, S. G. *Biophys. J.* **1987**, *51*, 937-946.

(36) McDermott, A.; Zysmilich, M. G.; Polenova, T. *Solid State Nucl. Mag. Res.* **1998**, *11*, 21-47.

(37) Matysik, J.; Alia; Hollander, J. G.; Egorova-Zachernyuk, T.; Gast, P.; de Groot, H. J. M. *Indian J. Biochem. Biophys.* **2000**, *37*, 418-423.

(38) Bennett, A. E.; Rienstra, C. M.; Auger, M.; Lakshmi, K. V.; Griffin, R. G. *J. Chem. Phys.* **1995**, *103*, 6951-6958.

(39) Daviso, E.; Diller, A.; Alia, A.; Matysik, J.; Jeschke, G. *J. Magn. Reson.* **2008**, *190*, 43-51.

(40) Matysik, J.; Diller, A.; Roy, E.; Alia, A. *Photosynth. Res.* **2009**, *102*, 427-435.

(41) Hu, X. C.; Ritz, T.; Damjanovic, A.; Autenrieth, F.; Schulten. K. *Q. Rev. Biophys.* **2002**, *35*, 1.

(42) Hoff, A. J.; Deisenhofer, J. *Phys. Rep.* **1997**, *287*, 2.

(43) Lendzian, F.; Huber, M.; Isaacson, R. A.; Endeward, B.; Plato, M.; Bonigk, B.; Möbius, K.; Lubitz, W.; Feher, G. *Biochim. Biophys. Acta* **1993**, *1183*,v139.

(44) Lubitz, W.; Lendzian, F.; Bittl, R. *Acc. Chem. Res.* 2002, *35*, 313.

(45) Rautter, J.; Lendzian, F.; Lubitz, W.; Wang, S.; Allen, J. P. *Biochemistry* **1994**, *33*, 12077.

(46) Schulten, E. A.; Matysik, J.; Alia; Kiihne, S.; Raap, J.; Lugtenburg, J.; Gast, P.; Hoff, A. J.; de Groot, H. J. *Biochemistry* **2002**, *41*, 8708-17.

(47) Prakash, S.; Alia, A.; Gast, P.; de Groot, H. J.; Jeschke, G.; Matysik, J. *Biochemistry* **2007**, *46*, 8953-60.

(48) Diller, A.; Alia, A.; Gast, P.; Jeschke, G.; Matysik, J. In Energy from the sun (Allen, J.; Gantt, E.; Golbeck, J.; Osmond, B. eds.), Springer Dordrecht, pp. 55-58 (**2008**).

(49) Blankenship, R. E. *Photosynth. Res.* **1992**, 33, 91-111.

(50) Golbeck, J. H. *Proc. Natl. Acad. Sc**i. U**. S. A.* **1993**, 90, 1642-1646.

(51) Permentier, H.P.; Schmidt, K.A.; Kobayashi, M.; Akiyama, M.; Hager-Braun, C.; Neerken, S.; Miller, M.; Amesz, J., *Photosynth. Res.* **2000**, 64, 27-39.

(52) Takaichi, S.; Oh-Oka, H.; *Plant Cell Physiol.* **1999**, 40, 691-694.

(53) Kobayashi, M.; Oh-Oka, H.; Akutsu, S.; Akiyama, M.; Tominaga, K.; Kise, H.; Nishida, F.; Watanabe, T.; Amesz, J.; Koizumi, M.; Ishida, N.; Kano, H., *Photosynth. Res* **2000**, 63, 269-280.

(54) Nuijs, A.M.; Vasmel, H.; Joppe, H.L.P.; Duysens, L.N.M.; Amesz, J., *Biochim. Biophys. Acta**1985**, 807,* 24-34.

(55) Vassiliev, I.R.; Antonkine, M.L.; Golbeck, J.H., *Biochim. Biophys. Acta* **2001**, 1507, 139-160.

(56) Golbeck, J. *Photosyn. Res.* **2007**, *91*, 139-140.

(57) Brok, M.; Vasmel, H.; Horikx, J.T.G.; Hoff, A.J., *FEBS Lett.* **1986**, 194, 322-326.

(58) Kobayashi, M.; van de Meent, E.J.; Erkelens, C.; Amesz, J.; Ikegami, I.; Watanabe, T., *Biochim. Biophys. Acta* **1991***, 1057*, 89-96.

(59) van de Meent, E. J.; Kobayashi, M.; Erkelens, C.; Vanveelen, P. A.; Amesz, J.; Watanabe, T. *Biochim. Biophys. Acta* **1991**, *1058*, 356-362.

(60) Prince, R. C.; Gest, H.; Blankenship, R. E. *Biochim. Biophys. Acta* **1985**, *810*, 377-384.

(61) Kleinherenbrink, F.A.M.; Amesz, J., *Biochim. Biophys. Acta* **1993**, 1143, 77-83.

(62) Watanabe, T.; Kobayashi, M.; Hongu, A.; Nakazato, M.; Hiyama, T.; Murata, N., *FEBS Lett*. **1985,** 191, 252-256.

(63) Zouni, A.; Witt, H.T.; Kern, J.; Fromme, P.; Krauss, N.; Saenger, W.; Orth, P., *Nature* **2001**, 409, 739-743.

(64) Ferreira, K.N.; Iverson, T.M.; Maghlaoui, K.; Barber, J.; Iwata, S., *Science* **2004**, 303, 1831-1838.

(65) Webber, A.N.; Lubitz, W. *Biochim. Biophys. Acta* **2001**, *1507*, 61-79.

(66) Barber, J. *Quart. Rev. Biophys*,**2003**, 36, 71-89.

(67) Witt, H. T. *Photosynth. Res*. **2004**, 80, 85-107.